Cellular/Molecular

Regulation of Synapse Weakening through Interactions of the Microtubule Associated Protein Tau with PACSIN1

Philip Regan,[1] Scott J. Mitchell,[2] Seung-Chan Kim,[2] Younbok Lee,[2] Jee Hyun Yi,[1] Saviana A. Barbati,[2] Christopher Shaw,[2] and Kwangwook Cho[1,2]

[1]Henry Wellcome Laboratories for Integrative Neuroscience and Endocrinology, Bristol Medical School, Faculty of Health Sciences, University of Bristol, Bristol BS1 3NY, United Kingdom, and [2]UK-Dementia Research Institute, Department of Basic and Clinical Neuroscience, Maurice Wohl Clinical Neuroscience Institute, King's College London, London SE5 9NU, United Kingdom

Hyperphosphorylation of the microtubule associated protein tau (tau) is inextricably linked to several neurodegenerative diseases, collectively termed tauopathies, in which synapse dysfunction occurs through largely unidentified mechanisms. Our research aimed to uncover molecular mechanisms by which phosphorylation of tau (pTau) affects synapse function. Using combined molecular and electrophysiological analysis with in vitro genetic knock-in of phosphorylation mutant human tau in male rat CA1 hippocampal neurons, we show an interplay between tau and protein kinase C and casein kinase substrate in neurons protein 1 (PACSIN1) that regulates synapse function. pTau at serine residues 396/404 decreases tau:PACSIN1 binding and evokes PACSIN1-dependent functional and structural synapse weakening. Knock-down of tau or PACSIN1 increases AMPA receptor (AMPAR)-mediated current at extrasynaptic regions, supporting a role for these proteins in affecting AMPAR trafficking. The pTau-induced PACSIN1 dissociation may represent a pathophysiological regulator of synapse function that underlies tauopathy-associated synapse defects.

Key words: **Alzheimer's disease; AMPA receptor; PACSIN1; phosphorylation; synapse; Tau**

Significance Statement

Knowledge is still lacking for how hyperphosphorylation of tau and its effectors lead to synaptic and neuronal dysfunction. Our results provide crucial insight for this mechanistic understanding; we show that specific tau phosphorylation events modulate its protein interaction with PACSIN1 and thus elicits synapse weakening likely through PACSIN1-dependent regulation of AMPA receptor (AMPAR) trafficking. These findings develop our understanding of molecular events that may be relevant to cellular changes underpinning tauopathy-associated neurodegenerative diseases.

Introduction

Synapse loss is a widely recognized prodromal pathology of neurodegenerative tauopathies such as Alzheimer's disease where the microtubule associated protein tau becomes hyperphosphorylated and aggregated (Selkoe, 2002). Hyperphosphorylated forms of tau are sufficient to induce synapse destabilization (Di et al., 2016), indicating that synapse defects are a direct early outcome of tauopathy, although the causal mechanisms remain undefined.

Previous studies show that tau localizes to synapses and affects synapse function (Ittner et al., 2010; Ahmed et al., 2014; Frandemiche et al., 2014; Kimura et al., 2014; Regan et al., 2015, 2017). Knock-down of neuronal tau results in altered distribution of AMPA receptors (AMPARs; Suzuki and Kimura, 2017) and impaired interaction between AMPARs and AMPAR trafficking machinery (Regan et al., 2015). Furthermore, forms of synaptic plasticity dependent on AMPAR turnover are reported to require tau (Ahmed et al., 2014; Kimura et al., 2014). Together, these findings suggest that tau affects synapse function via effects on AMPAR turnover and/or trafficking, yet it is not clear how tau may regulate these mechanisms nor the direct consequences of tau phosphorylation for synapse function.

Our study sought to investigate molecular mechanisms by which phosphorylation of tau (pTau) affects synaptic function. We tested the hypothesis that pTau at serine 396/404 residues would specifically affect synapse function, given that blockade of this event prevents synapse weakening (Regan et al., 2015).

Received Dec. 14, 2020; revised May 28, 2021; accepted June 1, 2021.

Author contributions: K.C. designed research; P.R., S.J.M., S.-C.K., Y.L., J.H.Y., and S.A.B. performed research; Y.L. and C.S. contributed unpublished reagents/analytic tools; P.R., S.J.M., S.-C.K., and S.A.B. analyzed data; P.R. wrote the first draft of the paper; P.R., S.J.M., and K.C. edited the paper; P.R. wrote the paper.

P.R. and K.C. were supported by the Biotechnology and Biological Sciences Research Council. K.C., C.S., Y. L., S.J.M., S.-C.K., and S.A.B. were supported by the UK Dementia Research Institute, which receives its funding from DRI LTD, funded by the UK Medical Research Council, Alzheimer's Society, and Alzheimer's Research UK. J.H.Y. was supported by the UK-Korea Alzheimer's disease research consortium program under the Korea Ministry of Health and Welfare. K.C. was supported by the Wellcome Trust.

The authors declare no competing financial interests.

Correspondence should be addressed to Kwangwook Cho at kei.cho@kcl.ac.uk.

https://doi.org/10.1523/JNEUROSCI.3129-20.2021

Furthermore, we predicted that the tau-interacting protein kinase C and casein Kinase II substrate in neurons protein 1 (PACSIN1), an F-BAR and SH3-domain containing protein with established roles in AMPAR endocytosis (Widagdo et al., 2016), would be a likely molecular candidate connecting tau to synapse regulation. Our results show that pTau at serine 396/404 (1) decreases the interaction between tau and PACSIN1; and (2) leads to reduced synaptic AMPAR function and structural synapse weakening that are both dependent on PACSIN1. Furthermore, we show that knock-down of neuronal tau or PACSIN1 causes an increase in AMPAR current within extrasynaptic regions, supporting necessary roles for these proteins in affecting AMPAR trafficking. Together, our findings identify a synergistic role for tau and PACSIN1 in regulating synaptic function whereby specific tau phosphorylation triggers tau:PACSIN1 dissociation and weakens synaptic AMPAR-mediated transmission.

Materials and Methods

Animals

All procedures involving animals were conducted in accordance with the United Kingdom Animals Scientific Procedures Act, 1986. Male 7- and 1-d-old Wistar rats (Charles River) were used to prepare organotypic hippocampal slices and primary cultured neurons, respectively. All animal experiments were given ethical approval by the ethics committee of University of Bristol or King's College London (protocol reference U214; United Kingdom).

Organotypic hippocampal slices

Organotypic slices were cultured as previously described (Regan et al., 2015). All steps were conducted under sterile conditions. Briefly, rats were decapitated and their brains rapidly removed and placed into ice-cold dissecting medium containing: 238 mM sucrose, 2.5 mM KCl, 26 mM $NaHCO_3$, 1 mM NaH_2PO_4, 5 mM $MgCl_2$, 11 mM D-glucose, and 1 mM $CaCl_2$. Hippocampi were extracted and transverse hippocampal slices were cut and placed on sterile, semi-porous membranes (Merck Millipore) and stored at the interface between air and culture medium containing: 78.8% minimum essential medium with L-glutamine, 20% heat-inactivated horse serum, 30 mM HEPES, 26 mM D-glucose, 5.8 mM $NaHCO_3$, 2 mM $CaCl_2$, 2 mM $MgSO_4$, 70 μM ascorbic acid, and 1 μg ml^{-1} insulin (pH adjusted to 7.3 and 320–330 mOsm kg^{-1}), inside a humidified incubator at 35°C with a 5% CO_2-enriched atmosphere.

Biolistic transfection

Organotypic slices were biolistically transfected at days in vitro (DIV) 3-4 using the Helios Gene Gun system (Bio-Rad). A mixture of four different tau shRNA constructs (1:1:1:1 in pGFP-V-RS vector (OriGene Technologies) was used for tau silencing, as previously described (Kimura et al., 2014). PACSIN1 shRNA (GCAGCTACATTCACGTCTATC) was designed in-house and expressed under the control of the pENTR/U6 vector. Human PACSIN1 (GenBank: BC040228.1) was expressed in the pCMV-SPORT6 vector. The human PACSIN1 P437L mutant was generated in-house, using the Q5 Site-directed mutagenesis kit (NEB). cDNA for full-length human tau (2N4R) and associated pseudophosphorylation mutants were expressed in a pCI-neo vector and co-transfected with rat tau shRNA. Tau-PHF1E corresponds to tau pseudophosphorylated (mutated to glutamate) at serine residues 396 and 404. Tau-AT8E corresponds to tau pseudophosphorylated at serine residues 199 and 202 and threonine 205. Tau-40E corresponds to tau pseudophosphorylated at serine residues 199, 202, 214, 396, and 404 and threonine residues 205 and 212. Phospho-null mutant tau isoforms, tau-PHF1A and tau-AT8A, comprise mutations to alanine at the residues specified above.

Electrophysiological recordings

Whole-cell recordings of neurons from organotypic hippocampal slices took place at DIV6–DIV8. Slices in the recording chamber were perfused with a buffer solution containing 119 mM NaCl, 2.5 mM KCl, 4 mM $CaCl_2$, 4 mM $MgCl_2$, 26 mM $NaHCO_3$, 1 mM NaH_2PO_4, 11 mM glucose, 0.04 mM picrotoxin, and 0.01 mM 2-chloroadenosine, at 29–30°C, saturated with 95% O_2/5% CO_2. As necessary, a stimulating electrode was placed on the Schaffer collateral pathway. For analysis of synaptic currents, patch pipettes (4–6 MΩ) were back-filled with filling solution comprising 130 mM $CsMeSO_4$, 8 mM NaCl, 4 mM Mg-ATP, 0.3 mM Na-GTP, 0.5 mM EGTA, 10 mM HEPES and 6 mM QX-314, pH 7.2–7.3, 285–290 mOsm kg^{-1}. For analysis of whole-cell currents, filling solution comprising 135 mM K-gluconate, 10 mM HEPES, 0.5 mM EGTA, 2 mM Mg-ATP, 0.3 mM Na-GTP, and 8 mM NaCl was used. Only cells with an initial Rs <20 MΩ that was maintained at a level within 20% of that value until experiment completion were included for data analysis.

Data were filtered at 2 kHz and digitized at 20 kHz using a Multiclamp 700A amplifier. Data were recorded and online data analysis was performed using WinLTP software. Offline data analysis was performed with WinLTP and Stimfit software.

Assays of extrasynaptic receptor-mediated current

To assay whole-cell AMPAR-mediated current, dual-patched neurons were voltage clamped at −60 mV. 500 nM TTX and 25 μM D-AP5 were added to the perfusion buffer, and the holding current was monitored (only cells with an initial holding current <100 pA were used). After a 5-min stable baseline, 500 nM AMPA and 10 μM cyclothiazide (CTZ) were perfused onto the slice. After 10 min AMPA perfusion, baseline buffer was restored and recordings were continued for a further 5 min. To assay whole-cell NMDA receptor (NMDAR)-mediated current, neurons were voltage clamped at −60 mV and perfused with a buffer containing 500 nM TTX and 10 μM NBQX. After a 5-min stable baseline, 10 μM NMDA was perfused onto the slice for 5 min, after which baseline buffer was restored for a further 5 min. The maximum change in the holding current elicited during AMPA or NMDA perfusion was quantified and compared between neurons.

To assay extrasynaptic AMPARs, a previously described method was adapted (Takayasu et al., 2004). Dual-patched neurons were voltage clamped at −70 mV and a burst stimulation (five pulses at 75 Hz), repeated every 30 s, was applied to the Schaffer Collateral pathway. After a 5-min baseline 50 μM D-AP5, 10 μM MK-801, and 10 μM UBP304 were added to the buffer solution to inhibit NMDAR-mediated and KAR-mediated EPSCs, thus isolating AMPAR currents. Stimulation was continued for a further 10 min, before 30 μM of the glutamate transporter blocker, DL-TBOA was added to the buffer solution to facilitate glutamate spillover to extrasynaptic regions. Stimulation was then continued for a further 15 min. In some experiments, 20 μM NBQX or 50 μM GYKI 53655 were added at the end to confirm that the EPSC was being mediated solely by AMPARs.

Extrasynaptic current analysis

The final 10 EPSCs recorded after DL-TBOA application were averaged to form a single EPSC waveform and the decay phase was best fit to a double exponential function, of the form $A(t) = A1e(-t/\tau1) + A2e(-t/\tau2)$, where A(t) is the amplitude A of the decay phase as a function of time (t), A1 and A2 are the amplitudes of the fast and slow decay components, respectively, and $\tau1$ and $\tau2$ are their time constants. The proportion of slow decay component was calculated as $A2/(A1 + A2) \times 100$, and this was compared across transfected and untransfected neurons. A value for weighted tau was calculated as $(A1\tau1 + A2\tau2)/(A1 + A2)$.

For graphical representation, all raw EPSCs were transformed and scaled relative to the peak amplitude of the EPSC after the final pulse (set as 100%) and the baseline holding current (set as 0%). Transformed EPSCs were averaged, and plotted as the mean ± SEM.

GST pulldown

HEK 293T cells were transfected with tau-GFP using Lipofectamine 2000 and lysate collected in RIPA buffer 48 h later. For the pulldown, 500 µg of precleared protein lysate was combined with 50 µl of Glutathione Sepharose beads (GE Healthcare, 17-0756-01) and 15 µg of GST only, GST-PACSIN1 wild-type (WT), or GST-PACSIN1 P437L. Bound proteins were subsequently eluted from the GST-beads complex in sample buffer and their presence analyzed by SDS-PAGE gel electrophoresis. The following primary antibodies were used for immunoblotting: mouse anti-

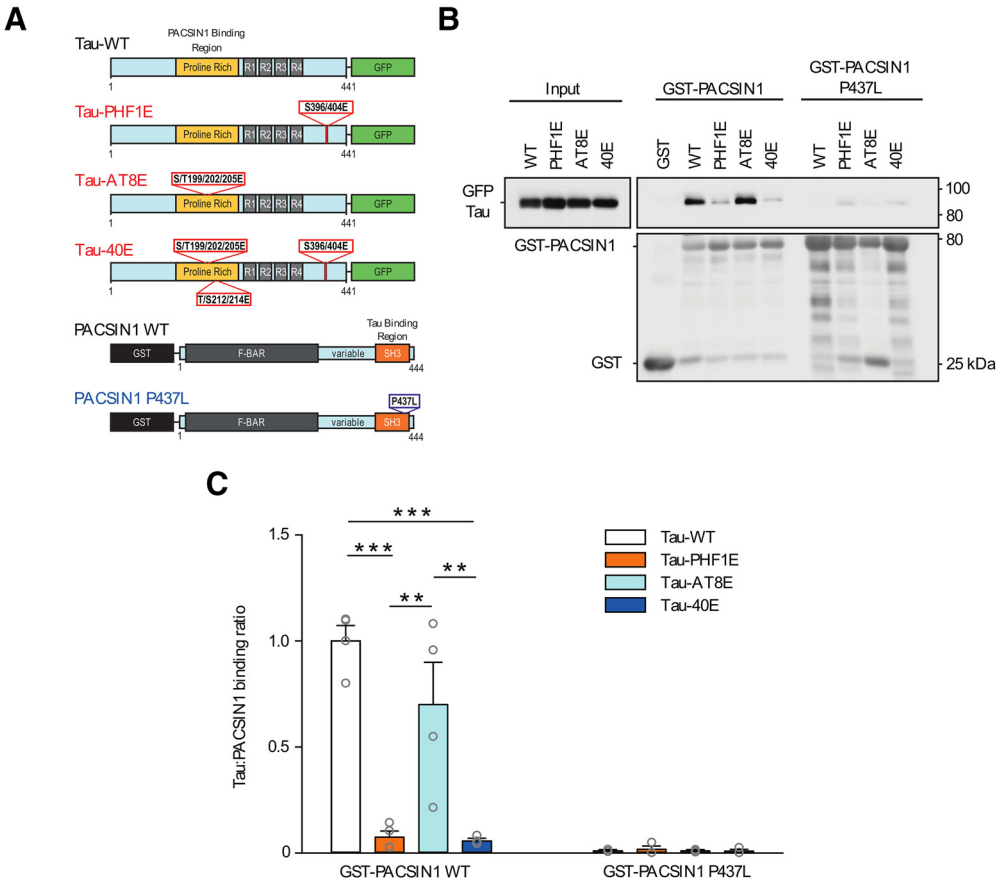

Figure 1. Tau phosphorylation regulates the association between tau and PACSIN1. ***A***, Molecular domains and pseudophosphorylation sites of Tau-GFP (top) and GST-PACSIN1 (bottom). ***B***, Representative western blot of Tau-GFP (WT, PHF1E, AT8E, 40E) pulldown with GST-PACSIN1 WT or P437L. ***C***, Quantification of tau:PACSIN1 binding ratio relative to averaged WT ($n = 4$; $p < 0.001$, one-way ANOVA with Bonferroni's *post hoc* test). Values for individual replicates are overlaid in circles, bars show mean ± SEM; $^{**}p < 0.01$, $^{***}p < 0.005$.

GFP (1:200; Santa Cruz sc-9996, RRID:AB_627695) and goat anti-GST (1:15 000; Abcam ab6613, RRID:AB_305594).

Multiphoton imaging

Transfected neurons in organotypic hippocampal slices were imaged at DIV7–DIV8, 3–4 d after transfection. Slices were submerged in HBS buffer and images were acquired using a Leica SP8 AOBS microscope together with a Spectra Physics DeepSee dual beam excitation laser and an external HyD detector (Wolfson Bioimaging Facility, Bristol University) and Scientifica Hyperscope with a Coherent Chameleon Discovery multiphoton laser (UK DRI Laboratory, King's College London). Z-stack images of dendritic spines were taken from apical dendrites, 100 µm from the soma. ROIs from secondary and tertiary dendritic branches (dendritic width ~0.8 µm) were isolated and spine density and morphology was analyzed using ImageJ software. Briefly, images were converted to 8-bit, and background subtracted followed by threshold adjustment. Dendritic segments were straightened and maximum z projections were obtained, and spines were counted using the Cell Counter ImageJ plugin and classified according to their morphology (stubby: length <1 µm, head width/neck width ratio <1.5; thin: length <1–5 µm, head width/neck width ratio <1.5; mushroom: length <5 µm, head width/neck width ratio >1.5). Images were acquired from three to five cells per condition per culture, across three to five separate cultures.

Other plasmids and transfection methods

For pulldown experiments, tau cDNA was cloned into a pcDNA3.1 vector, with C-terminally tagged GFP. Human PACSIN1 and PACSIN1 P437L cDNA were cloned into the pGEX-4T1 vector and protein expression was induced in Rosetta DE3 competent cells (Merck Millipore). All constructs were verified by Sanger sequencing. Rat tau and PACSIN1 shRNA sequences were also cloned into pLKO.1-GFP vectors and lentiviral transduction of primary cultured neurons at DIV7–DIV12 was used to verify protein knock-down.

Experimental design and statistical analyses

Statistical analysis was performed using IBM SPSS 23.0 software. Data groups were assessed for normal distribution using the Shapiro–Wilk test and for equal variance with Levene's test. Details of individual statistical tests are provided within relevant Results sections and figure legends. For most analyses, independent two-tailed *t* tests were performed, with an α level of 0.05. For comparisons of effects across multiple independent groups, one-way ANOVAs were performed followed by *post hoc* tests as described. Sample sizes are described in figure legends and were based on preliminary findings of the minimum number of samples that could be used to detect statistically significant differences in the group means, given the observed variance within groups at a power level of 0.8. Grouped data are presented as mean ± SEM. All data are available from the corresponding author, on request.

Results

Tau phosphorylation regulates its association with PACSIN1 and elicits functional synapse weakening

Knock-down of neuronal tau prevents synapse weakening (Kimura et al., 2014), although the mechanism by which tau affects synapse function in this manner has not been determined. A previous study in tau knock-out mice revealed an impaired association between AMPARs and protein interacting with protein kinase C (PICK1; Regan et al., 2015), indicating that tau somehow affects protein associations that control AMPAR

trafficking. We identified PACSIN1 as a possible intermediary between tau and AMPAR trafficking machinery. PACSIN1 directly binds to the proline rich domain of tau via its SH3 domain (Liu et al., 2012) and is also known to be required for AMPAR endocytosis via multiple interactions of its SH3 and F-BAR domains, including with PICK1 (Liu et al., 2012; Anggono et al., 2013; Widagdo et al., 2016).

We predicted that the interaction and modulation of tau: PACSIN1 binding may therefore be important regulators of AMPAR trafficking. Since pTau is required for synaptic AMPAR weakening (Regan et al., 2015), it was of interest whether pTau affects its interaction with PACSIN1. This was investigated using GST-tagged PACSIN1 to immunoprecipitate different phosphomutant GFP-tagged tau isoforms expressed in HEK293T cells. We compared binding of PACSIN1 to WT full-length human tau (2N4R) and three different phosphomutant isoforms (PHF1E, AT8E, 40E; Fig. 1*A*) as well as binding of the different tau isoforms to a mutant form of human PACSIN1 (P437L) unable to bind tau (Liu et al., 2012). GST-PACSIN1 robustly bound to WT-tau, consistent with previous findings (Liu et al., 2012; Fig. 1*B*,*C*) and this interaction was affected by the phosphorylation status of tau ($F_{(3,12)} = 19.51$, $p < 0.001$, one-way ANOVA). Tau-PHF1E (pseudophosphorylated at serine 396/404) vastly reduced the interaction between tau and GST-PACSIN1, whereas tau-AT8E (pseudophosphorylated at serine/threonine 199/202/205) had no significant effect (Fig. 1*B*,*C*). Combined pseudophosphorylation of the above residues (tau-40E) also strongly reduced binding to GST-PACSIN1. As expected, interactions between all tau isoforms and GST-PACSIN1 P437L were effectively abolished (Fig. 1*B*,*C*). Together, our findings demonstrate that pTau at serine 396/404 has a dominant negative effect on tau:PACSIN1 binding, suggesting that pTau at these residues (e.g., during synaptic plasticity; Regan et al., 2015) may act as a trigger for tau:PACSIN1 dissociation.

Tau hyperphosphorylation is correlated with cognitive decline and synapse loss in neurodegenerative disease (Jadhav et al., 2015; Di et al., 2016) and previous studies suggest that pTau may have a role in weakening of synapses in neurons (Hoover et al., 2010; Regan et al., 2015). However, whether there is a direct causal link between these synaptic effects and pTau is not known, nor whether distinct phosphorylation events on tau are sufficient to induce synapse weakening. To test this, CA1 neurons of organotypic rat hippocampal slices were co-transfected with rat sh-Tau that suppressed endogenous tau expression ($t_{(12)} = 5.35$, $p < 0.001$, unpaired *t* test; Fig. 2*A*,*B*) and cDNA for PHF1E or AT8E pseudophosphorylated human tau. We found a significant reduction of $EPSC_{AMPA}$ ($t_{(42)} = 3.29$, $p = 0.002$, unpaired *t* test) but not $EPSC_{NMDA}$ ($t_{(32)} = 0.73$, $p = 0.47$, unpaired *t* test) in neurons expressing tau-PHF1E (Fig. 2*C*). No changes to $EPSC_{AMPA}$ ($t_{(38)} = 0.67$, $p = 0.51$, unpaired *t* test) or $EPSC_{NMDA}$ ($t_{(38)} = 0.20$, $p = 0.84$, unpaired *t* test) were present in neurons expressing tau-AT8E (Fig. 2*D*). Similarly, no changes in $EPSC_{AMPA}$ were present in neurons transfected with equivalent phospho-null mutants, tau-PHF1A (AMPA: $t_{(34)} = 1.01$, $p = 0.32$; NMDA: $t_{(32)} = 1.99$, $p = 0.06$, unpaired *t* test) or tau-AT8A (AMPA: $t_{(38)} = 1.55$, $p = 0.13$; NMDA: $t_{(36)} = 1.18$, $p = 0.25$, unpaired *t* test), indicating that reduced $EPSC_{AMPA}$ is directly related to the phosphorylation status of tau-PHF1E (Fig. 2*E*,*F*). We predicted that pTau would promote synapse weakening via a mechanism involving PACSIN1. To test this, endogenous PACSIN1 levels were suppressed with transfection of PACSIN1 shRNA (sh-PACSIN1: $t_{(11)} = 4.24$, $p < 0.001$, unpaired *t* test; Fig. 2*G*,*H*), which by itself did not affect measures of synaptic current (AMPA: $t_{(54)} = 0.75$, $p = 0.456$; NMDA: $t_{(30)} = 0.31$, $p = 0.758$, unpaired *t* test; Fig. 2*I*). In support of our hypothesis, when tau-PHF1E was co-transfected with rat sh-PACSIN1 no significant changes in $EPSC_{AMPA}$ or $EPSC_{NMDA}$ were observed compared with untransfected neurons (AMPA: $t_{(44)} = 1.69$, $p = 0.10$; NMDA: $t_{(44)} = 0.75$, $p = 0.46$, unpaired *t* test; Fig. 2*J*). These data indicate that pTau at serine 396/404 specifically reduces synaptic AMPAR-mediated transmission in a PACSIN1-dependent manner.

Tau knock-down increases extrasynaptic AMPAR-mediated current

Our data and those of others support a model whereby tau, specifically pTau, regulates synaptic function through effects on AMPAR trafficking mechanisms (Regan et al., 2015; Suzuki and Kimura, 2017). Given that pTau reduces synaptic AMPAR currents, we predicted that tau knock-down might increase AMPAR currents, perhaps through impaired basal association of AMPARs with protein trafficking complexes. To determine whether tau affects the basal surface expression of AMPARs, we compared surface AMPAR function in tau knock-down neurons using bath perfusion of the AMPAR-agonist, (*RS*)-AMPA, which activates all surface AMPARs. In this assay, the change in holding current of a voltage-clamped neuron provides a measure of the amount of current elicited through agonist activation of AMPARs. Sh-Tau was used to knock-down tau expression in biolistically transfected CA1 neurons. Grouped data showed an enhanced holding current response to AMPA in sh-Tau neurons compared with untransfected neurons ($t_{(19)} = 2.67$, $p = 0.015$, unpaired *t* test; Fig. 3*A*,*B*). In contrast, no differences in response to bath perfusion of the NMDAR agonist, NMDA, were observed ($t_{(21)} = 1.52$, $p = 0.144$, unpaired *t* test; Fig. 3*C*,*D*). No significant differences in measures of series and input resistance were observed between control and experimental groups during these assays ($p > 0.05$, unpaired *t* tests). These data support the notion that tau knock-down affects AMPAR trafficking mechanisms leading to surface AMPAR accumulation.

Our whole-cell current data showing increased surface AMPAR current in sh-Tau neurons contrasts somewhat with previous data showing unaltered evoked basal synaptic transmission in neurons lacking tau, including our own data in which sh-Tau neurons were measured under directly comparable experimental conditions to those here (Kimura et al., 2014; Regan et al., 2015). However, given that localized zones of AMPAR surface trafficking are prevalent within extrasynaptic regions (Rácz et al., 2004), we predicted that tau knock-down might instead increase AMPAR-mediated transmission primarily in extrasynaptic pools rather than at the synapse. Extrasynaptic AMPAR-mediated current was therefore analyzed using combined pharmacological and electrical stimulation. Briefly, EPSCs ($EPSC_{AMPA}$) were recorded during whole-cell voltage clamp and the extrasynaptic component of $EPSC_{AMPA}$ was assayed following synaptic glutamate spillover induced by the glutamate uptake inhibitor DL-threo-β-benzyloxyaspartate (TBOA). To quantify extrasynaptic $EPSC_{AMPA}$, we analyzed the decay phase of EPSCs by fitting them to an exponential function. Exponential curve fitting of EPSC decay enables fast and slow components of the current to be resolved, which can reflect activation kinetics of distinct subpopulations of AMPARs (Takayasu et al., 2004; Stincic and Frerking, 2015). EPSC decay after TBOA treatment was best fit by a biexponential decay function, reflecting the activation of a fast synaptic and slower extrasynaptic component of EPSC decay. Weighted time constants (τ_w) of decay were significantly

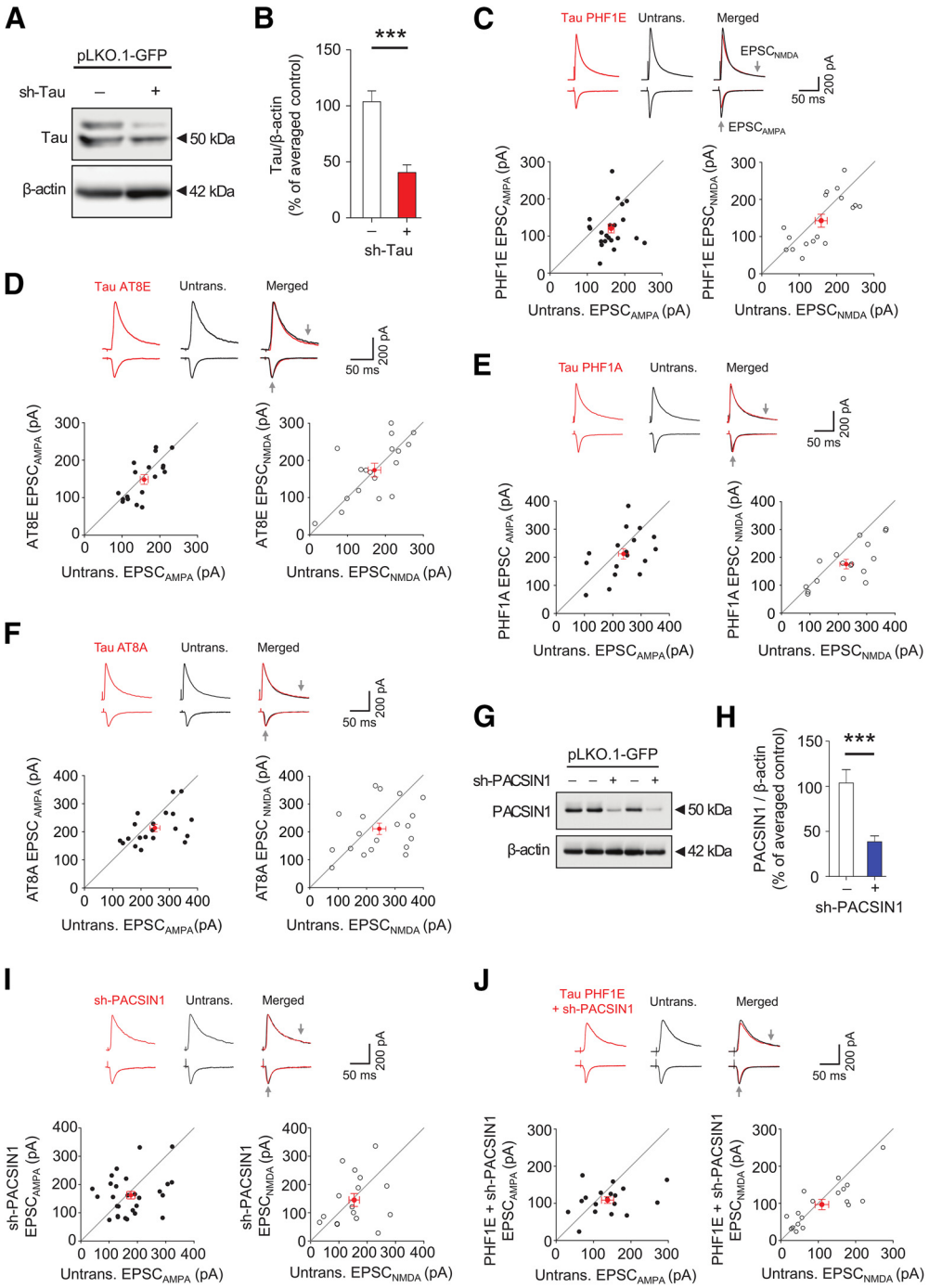

Figure 2. Tau phosphorylation induces PACSIN1-dependent functional synapse weakening. Representative Western blotting (***A***) and quantification (***B***) of tau expression in control and sh-Tau transduced primary neurons ($n = 7$ from 4 biological replicates). ***C***, Amplitudes of (left) $EPSC_{AMPA}$ ($n = 22$) and (right) $EPSC_{NMDA}$ ($n = 17$) in pairs of untransfected and tau-PHF1E transfected neurons. ***D***, Amplitudes of (left) $EPSC_{AMPA}$ and (right) $EPSC_{NMDA}$ in pairs of untransfected and tau-AT8E transfected neurons ($n = 20$). ***E***, Amplitudes of (left) $EPSC_{AMPA}$ ($n = 18$; $p = 0.32$, unpaired t test) and (right) $EPSC_{NMDA}$ ($n = 17$; $p = 0.055$, unpaired t test) in pairs of untransfected and Tau-PHF1A transfected neurons. ***F***, Amplitudes of (left) $EPSC_{AMPA}$ ($n = 20$; $p = 0.13$, unpaired t test) and (right) $EPSC_{NMDA}$ ($n = 19$; $p = 0.25$, unpaired t test) in pairs of untransfected and Tau-AT8A transfected neurons. Representative Western blotting (***G***) and quantification (***H***) of PACSIN1 protein expression levels in control and sh-PACSIN1 transduced primary neurons. ***I***, Amplitudes of (left) $EPSC_{AMPA}$ ($n = 28$; $p = 0.456$, unpaired t test) and (right) $EPSC_{NMDA}$ ($n = 16$; $p = 0.758$, unpaired t test) in pairs of untransfected and sh-PACSIN1 transfected neurons. ***J***, Amplitudes of (left) $EPSC_{AMPA}$ and (right) $EPSC_{NMDA}$ in pairs of untransfected and tau-PHF1E and sh-PACSIN1 co-transfected neurons ($n = 23$). EPSC representative traces recorded at the different holding voltages are provided inset with peak amplitude measurements indicated by gray arrows. All electrophysiology data shown in panels ***C–F***, ***I***, ***J*** are obtained from organotypic hippocampal slice preparations. Values for individual cell pairs are overlaid in circles, bars show mean ± SEM; $^{***}p < 0.005$.

slower for sh-Tau neurons compared with untransfected neurons after TBOA treatment ($t_{(22)} = 2.43$, $p = 0.024$, unpaired t test; Fig. 3*E*,*F*). The proportion of slow decay was also larger in sh-Tau neurons compared with untransfected neurons ($t_{(22)} = 2.32$, $p = 0.034$, unpaired t test; Fig. 3*F*), together suggesting that prolonged decay of EPSCs following glutamate spillover in sh-Tau neurons is because of an increased delayed current component, i.e., a larger extrasynaptic subpopulation of AMPARs. These data

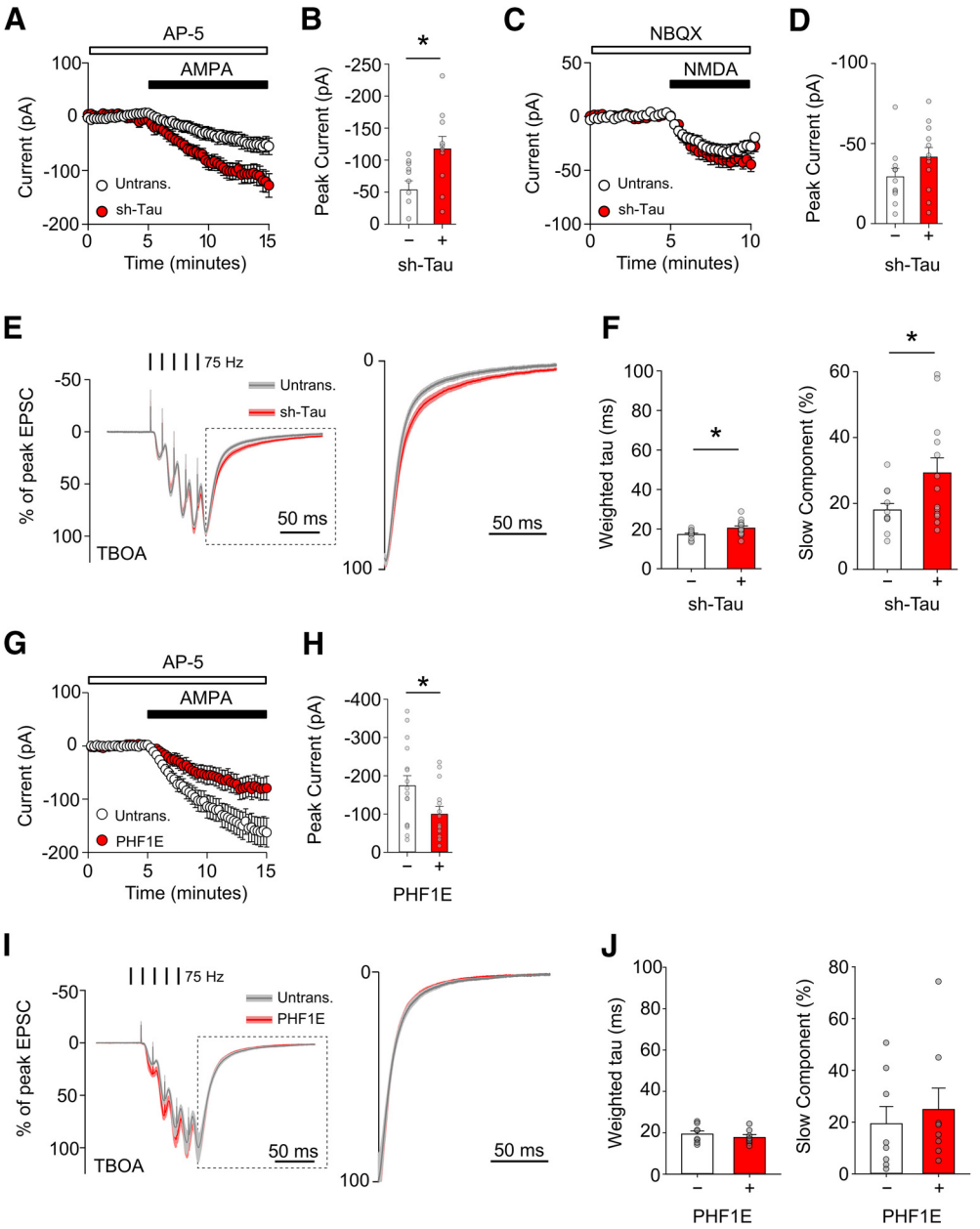

Figure 3. Increased surface AMPAR levels in sh-Tau transfected neurons. Changes over time (***A***) and maximum change (***B***) in whole-cell holding current for untransfected ($n = 11$) and sh-Tau neurons ($n = 10$) during AMPA perfusion. Changes over time (***C***) and maximum change (***D***) in whole-cell holding current for untransfected ($n = 11$) and sh-Tau neurons ($n = 12$) during NMDA perfusion. ***E***, left, Scaled EPSCs (lines showing mean/SEM) after TBOA during 75-Hz stimulation. Right, Enlarged EPSC decay. ***F***, Weighted tau (left) and slow component (right) of EPSC decay post-TBOA from untransfected ($n = 11$) and sh-Tau ($n = 13$) neurons during 75-Hz stimulation. Changes over time (***G***) and maximum change (***H***) in whole-cell holding current for untransfected ($n = 16$) and tau-PHF1E transfected neurons ($n = 14$) during (*RS*)-AMPA perfusion. ***I***, left, Scaled EPSCs (lines showing mean/SEM) after TBOA during 75-Hz stimulation of tau-PHF1E and untransfected neurons. Right, Enlarged EPSC decay. ***J***, Weighted tau and slow component of EPSC decay post-TBOA from untransfected ($n = 8$) and tau-PHF1E ($n = 8$) neurons during 75-Hz stimulation. All data are obtained from organotypic hippocampal slice preparations. Values for individual neurons are overlaid in gray circles, bars and symbols show mean ± SEM; $^*p < 0.05$.

support our hypothesis that tau knock-down increases AMPAR-mediated transmission within extrasynaptic domains. We also analyzed extrasynaptic current in tau-PHF1E cells, which displayed a marked reduction in holding current response to bath-applied AMPA when compared with untransfected neurons ($t_{(28)} = 2.17$, $p = 0.04$, unpaired *t* test; Fig. 3*G*,*H*). However, no differences in $EPSC_{AMPA}$ decay kinetics were observed in tau-PHF1E cells following TBOA-induced glutamate spillover (weighted tau: $t_{(14)} = 0.84$, $p = 0.42$, unpaired *t* test; slow component %: $t_{(14)} = 0.52$, $p = 0.61$, unpaired *t* test; Fig. 3*I*,*J*), indicating that the reduction in surface AMPARs in tau-PHF1E neurons manifests primarily in synaptic (Fig. 2*C*), rather than extrasynaptic domains.

PACSIN1 knock-down increases extrasynaptic AMPAR function

Our data indicate that PACSIN1 is required for the synapse weakening effects of pTau on AMPAR currents, potentially reflective of a role for PACSIN1 in signaling between tau and AMPAR trafficking mechanisms. We therefore predicted that the effects of PACSIN1 knock-down would phenocopy the effects of tau knock-down on surface AMPAR mediated synaptic

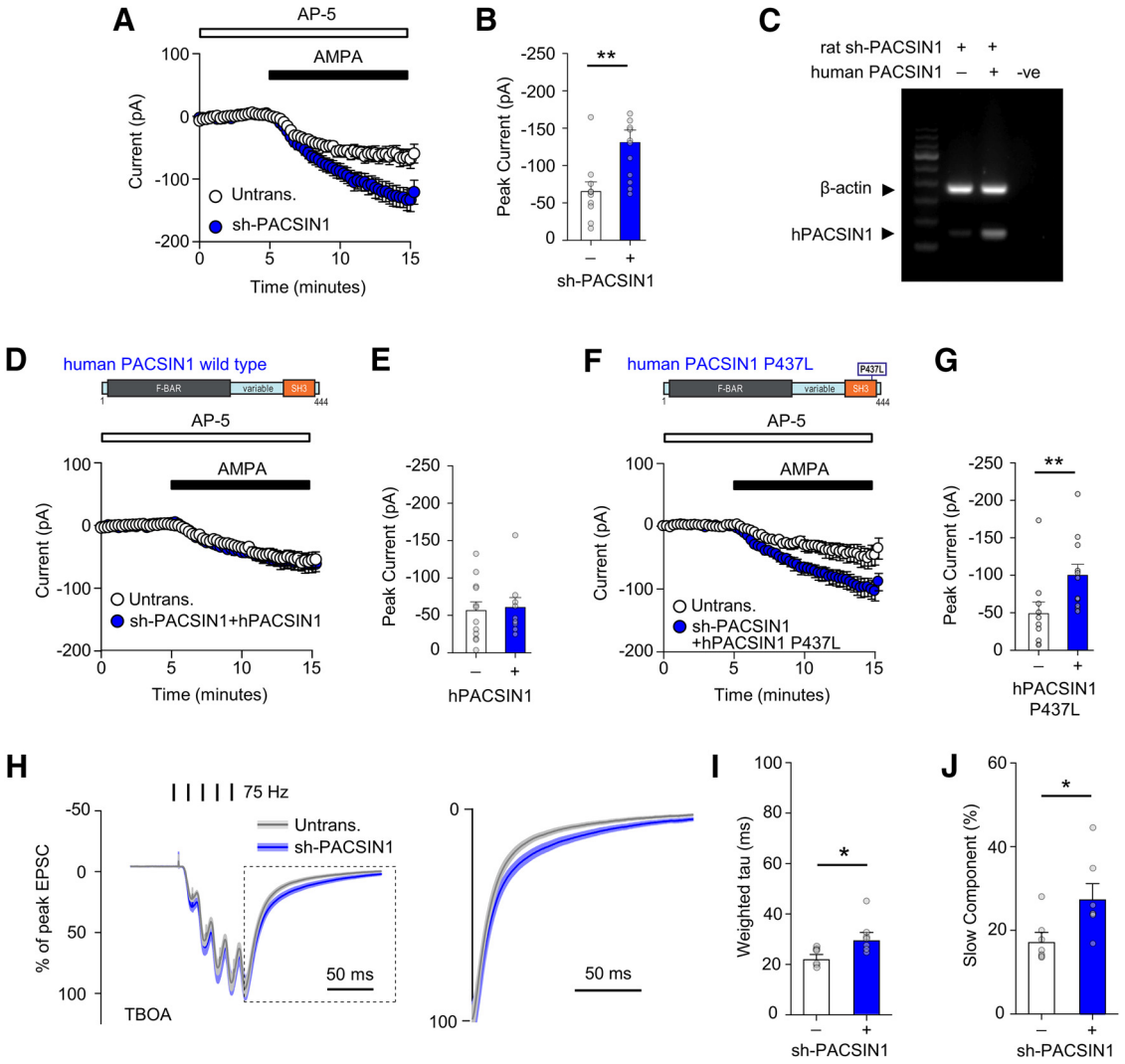

Figure 4. Increased surface AMPAR levels in sh-PACSIN1 transfected neurons. Changes over time (***A***) and maximum change (***B***) in whole-cell holding current for untransfected ($n = 10$) and sh-PACSIN1 transfected neurons ($n = 12$) during (*RS*)-AMPA perfusion. ***C***, Single-cell PCR assay confirming the expression of human PACSIN1 (hPACSIN1) in sh-PACSIN1 and hPACSIN1 co-transfected neurons. Changes over time (***D***) and maximum change (***E***) in whole-cell holding current for untransfected ($n = 12$) and sh-PACSIN1 and hPACSIN1 co-transfected neurons ($n = 9$) during (*RS*)-AMPA perfusion. Changes over time (***F***) and maximum change (***G***) in whole-cell holding current for untransfected ($n = 10$) and sh-PACSIN1 and hPACSIN1 P437L co-transfected neurons ($n = 11$) during (*RS*)-AMPA perfusion. ***H***, left, Scaled EPSCs (lines showing mean/*SEM*) after TBOA during 75-Hz stimulation of sh-PACSIN1 and untransfected neurons. Right, Enlarged EPSC decay. Weighted tau (***I***) and slow component (***J***) of EPSC decay post-TBOA from untransfected ($n = 7$) and sh-PACSIN1 ($n = 7$) neurons during 75-Hz stimulation. All data are obtained from organotypic hippocampal slice preparations. Values for individual neurons are overlaid in gray circles, bars and symbols show mean ± SEM; $^*p < 0.05$, $^{**}p < 0.01$.

transmission. Recordings of biolistically transfected CA1 neurons revealed that sh-PACSIN1 neurons exhibit an enhanced holding current response to bath-applied AMPA ($t_{(20)} = 2.99$, $p = 0.007$, unpaired *t* test; Fig. 4*A*,*B*). Rescue of PACSIN1 expression by co-transfection of shRNA-resistant human PACSIN1 (Fig. 4*C*) restored the AMPA-induced holding current change to control levels ($t_{(19)} = 0.24$, $p = 0.815$, unpaired *t* test; Fig. 4*D*,*E*). In contrast, expression of the SH3-domain mutant PACSIN1 (P437L) failed to reverse the sh-PACSIN1 effect on AMPA-induced current ($t_{(19)} = 2.40$, $p = 0.027$, unpaired *t* test), consistent with evidence that SH3-domain interactions of PACSIN1 are necessary for AMPAR internalization (Widagdo et al., 2016; Fig. 4*F*, *G*). Similar to the effects of tau knock-down, sh-PACSIN1 neurons exhibit a slower decaying current ($t_{(13)} = 2.596$, $p = 0.023$, unpaired *t* test) and larger slow component of decay ($t_{(13)} = 2.562$, $p = 0.025$, unpaired *t* test) compared with untransfected neurons following TBOA-induced glutamate spillover (Fig. 4*H–J*) indicative of a larger extrasynaptic subpopulation of AMPARs. The overall data suggest that PACSIN1 and tau mediate common effects on AMPAR trafficking, such that their reduced expression causes an accumulation and thus increased AMPAR-mediated transmission specifically within extrasynaptic domains.

Tau phosphorylation causes PACSIN1-dependent structural synapse weakening

Since dendritic spine number and structure is tightly associated with excitatory synapse function (Kasai et al., 2010; Hayashi-Takagi et al., 2015) and correlates with synaptic AMPAR content (Matsuzaki et al., 2001), we investigated whether pTau also induces structural weakening of synapses. No changes to spine density compared with GFP-transfected neurons were observed with either tau-PHF1E or tau-AT8E neurons ($F_{(4,45)} = 2.23$, $p = 0.08$, one-way ANOVA; Fig. 5*A*,*B*). However, a significant effect of pTau status was observed on morphology of dendritic spines (stubby: $F_{(4,57)} = 5.28$, $p = 0.001$; thin: $F_{(4,57)} = 5.77$, $p < 0.001$; mushroom: $F_{(4,57)} = 20.9$, $p < 0.0001$, one-way ANOVA). No

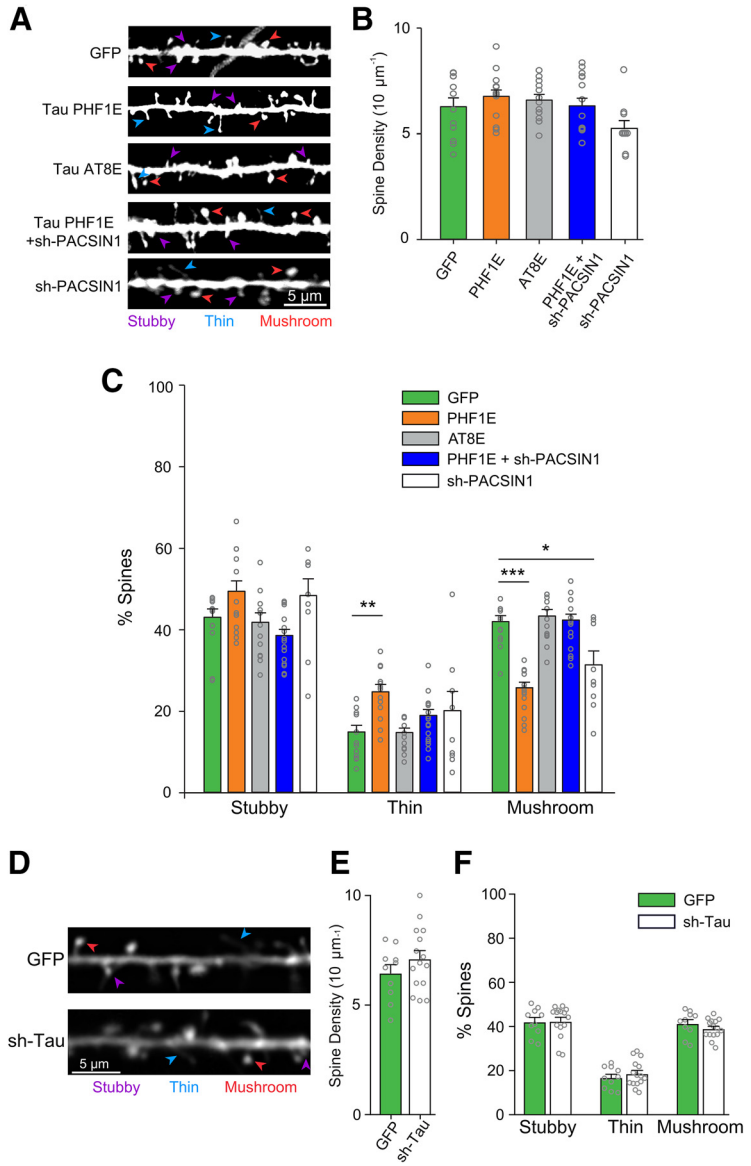

Figure 5. Tau phosphorylation induces PACSIN1-dependent structural synapse weakening. ***A***, Representative thresholded images of apical dendritic regions of interest from transfected CA1 neurons of hippocampal organotypic slices. Arrowheads indicate example stubby, thin, and mushroom spines. ***B***, Quantified spine density in GFP ($n = 12$ cells/9 slices/3 animals), tau-PHF1E ($n = 14$ cells/13 slices/5 animals), tau-AT8E ($n = 12$ cells/9 slices/5 animals), tau PHF1E + sh-PACSIN1 ($n = 16$ cells/9 slices/4 animals), and sh-PACSIN1 ($n = 10$ cells/5 slices/4 animals) transfected neurons. ***C***, Percentage of spines classified into stubby, thin and mushroom spines across transfection conditions (stubby: $p = 0.001$; thin: $p < 0.001$; mushroom: $p < 0.0001$, one-way ANOVA with *post hoc* Dunnett's test). ***D***, Representative images of apical dendritic regions of interest from transfected CA1 neurons of hippocampal organotypic slices. Arrowheads indicate example stubby, thin and mushroom spines. ***E***, Quantified spine density in GFP ($n = 10$ cells/8 slices/4 animals) and sh-Tau ($n = 15$ cells/10 slices/5 animals) transfected neurons. ***F***, Percentage of spines classified into stubby, thin and mushroom spines (stubby: $p = 0.93$; thin: $p = 0.78$; mushroom: $p = 0.26$, unpaired t tests). All data are obtained from organotypic hippocampal slice preparations. Values for individual cells are overlaid in gray circles, bars show mean ± SEM; $^{*}p < 0.05$, $^{**}p < 0.01$, $^{***}p < 0.005$.

significant difference in group means were detected relative to GFP-transfected neurons for stubby spines during *post hoc* analysis; however, there was a significant increase in the proportion of thin spines, and a significant reduction in the proportion of mushroom spines in tau-PHF1E neurons compared with GFP neurons, indicative of structural synapse weakening (Fig. 5*C*). No changes to spine morphology were observed in tau-AT8E neurons compared with GFP neurons (Fig. 5*C*). Importantly, in a separate set of experiments, sh-Tau alone also had no effect on dendritic spine density ($t_{(23)} = 1.17$, $p = 0.26$, unpaired t test) or structure (stubby: $t_{(23)} = 0.09$, $p = 0.93$; thin: $t_{(23)} = 0.78$, $p = 0.44$; mushroom: $t_{(23)} = 1.16$, $p = 0.26$, unpaired t tests; Fig. 5*D–F*), indicating that changes to spine phenotype are directly related to the overexpression of tau-PHF1E in this system. Consistent with our functional synapse assay, co-transfection of sh-PACSIN1 prevented the tau-PHF1E induced shift toward/away from thin/mushroom spines, respectively (Fig. 5*C*). We noted that sh-PACSIN1 transfection alone reduced mushroom spines (Fig. 5*C*), potentially a result of the role of PACSIN1 in modulating spine maturation (Schael et al., 2013). This effect, however, did not appear to modulate synaptic AMPAR currents (Fig. 2*I*). We predict that this data reflects the diversity of PACSIN1 function in physiological and pathophysiological conditions, whereby its multiple interactions converge on mechanisms of actin regulation that influence both receptor trafficking and cytoskeleton architecture. Overall, our data support a model in which a shift toward synapse weakening induced by overexpression of tau-PHF1E is mitigated by the reducing the expression of PACSIN1.

Discussion

Here, we demonstrate that the binding of tau to a regulator of AMPAR trafficking, PACSIN1, is affected by specific phosphorylation events on tau. Knock-down of either protein increases surface AMPAR function specifically within extrasynaptic sites. Phosphorylation of tau at serine 396/404 appears to drive a "gain of toxic function" involving reduced synaptic AMPAR function and structural synapse weakening that is mitigated by ablating PACSIN1.

PACSIN1 has multiple binding partners and it remains to be defined how its dissociation from tau fits within a regulatable mechanism of AMPAR trafficking. One possibility is that the pTau-induced dissociation of tau from PACSIN1 frees up the SH3 domain of PACSIN1 to interact with regulators of AMPAR trafficking such as dynamin or *N*-WASP (Widagdo et al., 2016). It is not clear, in this case, why knock-down of tau causes surface AMPAR accumulation. It could be that basal tau binding is required for the initial trafficking of PACSIN1 to the synapse, or for holding PACSIN1 in an "open" conformation that facilitates its dimerization and interactions of its F-BAR domain (Rao et al., 2010). These remain open questions worthy of future examination.

The increased surface AMPAR function following tau or PACSIN1 knock-down is consistent with synergistic effects on AMPAR trafficking mechanisms. Our observations of increased extrasynaptic AMPAR current in sh-Tau neurons match with findings that tau deletion increases intra-dendritic GluA2 levels

(Suzuki and Kimura, 2017). A previous study showed that neuronal PACSIN1 knock-down had no significant effect on steady-state surface AMPAR levels (Anggono et al., 2013), which contrasts with our results. We expect that differences between neuronal preparations and assay readouts likely explain the differences in observations. We predict that tau and PACSIN1 co-ordinate and effect signaling mechanisms culminating in AMPAR endocytosis, such that the knock-down of these proteins results in defective AMPAR endocytosis and thus surface AMPAR accumulation. However, we cannot discount alternative explanations for this accumulation, which may include increased AMPAR insertion or redistribution from synaptic sites where AMPAR anchoring may be reduced. We believe that these possibilities are unlikely, given that basal synaptic AMPAR currents and long-term potentiation (LTP), which rely on AMPAR insertion and synaptic anchoring (Opazo et al., 2012), are unaffected in tau knock-out neurons in our hands (Kimura et al., 2014; Regan et al., 2015). In contrast, long-term depression (LTD) is absent in tau knock-out neurons (Kimura et al., 2014), suggesting that defective endocytosis is the likely mechanism underlying our observations of increased surface AMPAR function. In this scenario, our data also highlight the importance of extrasynaptic sites for AMPAR internalization. Given that LTD manifests through surface AMPAR removal from extrasynaptic regions (Ashby et al., 2004), it is plausible that impaired internalization at these sites is responsible for absent LTD in tau knock-out neurons. Future experiments will be necessary to directly test our prediction that tau and PACSIN1 modulate synaptic and neuronal physiology through synergistic effects on AMPAR endocytosis.

Together, our findings highlight a molecular interplay between tau and PACSIN1 that may provide an important signaling mechanism underlying synaptic modulation during neuronal physiology. It will be hugely informative to study whether this interplay is directly dysregulated by hyperphosphorylated tau during early stages of tauopathies in the adult or aged brain, leading to aberrant synapse weakening. It is noteworthy that the specific pTau events described here are observed in physiological (Regan et al., 2015) and pathologic (Mondragón-Rodríguez et al., 2014) conditions, indicating that these phenomena and the dissociation of tau:PACSIN1 may have significant pathophysiological relevance for functional and structural synapse weakening in neurodegeneration.

References

Ahmed T, Van der Jeugd A, Blum D, Galas MC, D'Hooge R, Buee L, Balschun D (2014) Cognition and hippocampal synaptic plasticity in mice with a homozygous tau deletion. Neurobiol Aging 35:2474–2478.

Anggono V, Koç-Schmitz Y, Widagdo J, Kormann J, Quan A, Chen CM, Robinson PJ, Choi SY, Linden DJ, Plomann M, Huganir RL (2013) PICK1 interacts with PACSIN to regulate AMPA receptor internalization and cerebellar long-term depression. Proc Natl Acad Sci USA 110:13976–13981.

Ashby MC, De La Rue SA, Ralph GS, Uney J, Collingridge GL, Henley JM (2004) Removal of AMPA receptors (AMPARs) from synapses is preceded by transient endocytosis of extrasynaptic AMPARs. J Neurosci 24:5172–5176.

Di J, Cohen LS, Corbo CP, Phillips GR, El Idrissi A, Alonso AD (2016) Abnormal tau induces cognitive impairment through two different mechanisms: synaptic dysfunction and neuronal loss. Sci Rep 6:20833.

Frandemiche ML, De Seranno S, Rush T, Borel E, Elie A, Arnal I, Lanté F, Buisson A (2014) Activity-dependent tau protein translocation to excitatory synapse is disrupted by exposure to amyloid-beta oligomers. J Neurosci 34:6084–6097.

Hayashi-Takagi A, Yagishita S, Nakamura M, Shirai F, Wu YI, Loshbaugh AL, Kuhlman B, Hahn KM, Kasai H (2015) Labelling and optical erasure of synaptic memory traces in the motor cortex. Nature 525:333–338.

Hoover BR, Reed MN, Su J, Penrod RD, Kotilinek LA, Grant MK, Pitstick R, Carlson GA, Lanier LM, Yuan LL, Ashe KH, Liao D (2010) Tau mislocalization to dendritic spines mediates synaptic dysfunction independently of neurodegeneration. Neuron 68:1067–1081.

Ittner LM, Ke YD, Delerue F, Bi M, Gladbach A, van Eersel J, Wölfing H, Chieng BC, Christie MJ, Napier IA, Eckert A, Staufenbiel M, Hardeman E, Götz J (2010) Dendritic function of tau mediates amyloid-beta toxicity in Alzheimer's disease mouse models. Cell 142:387–397.

Jadhav S, Cubinkova V, Zimova I, Brezovakova V, Madari A, Cigankova V, Zilka N (2015) Tau-mediated synaptic damage in Alzheimer's disease. Transl Neurosci 6:214–226.

Kasai H, Fukuda M, Watanabe S, Hayashi-Takagi A, Noguchi J (2010) Structural dynamics of dendritic spines in memory and cognition. Trends Neurosci 33:121–129.

Kimura T, Whitcomb DJ, Jo J, Regan P, Piers T, Heo S, Brown C, Hashikawa T, Murayama M, Seok H, Sotiropoulos I, Kim E, Collingridge GL, Takashima A, Cho K (2014) Microtubule-associated protein tau is essential for long-term depression in the hippocampus. Philos Trans R Soc Lond B Biol Sci 369:20130144.

Liu Y, Lv K, Li Z, Yu AC, Chen J, Teng J (2012) PACSIN1, a Tau-interacting protein, regulates axonal elongation and branching by facilitating microtubule instability. J Biol Chem 287:39911–39924.

Matsuzaki M, Ellis-Davies GC, Nemoto T, Miyashita Y, Iino M, Kasai H (2001) Dendritic spine geometry is critical for AMPA receptor expression in hippocampal CA1 pyramidal neurons. Nat Neurosci 4:1086–1092.

Mondragón-Rodríguez S, Perry G, Luna-Muñoz J, Acevedo-Aquino MC, Williams S (2014) Phosphorylation of tau protein at sites Ser(396-404) is one of the earliest events in Alzheimer's disease and Down syndrome. Neuropathol Appl Neurobiol 40:121–135.

Opazo P, Sainlos M, Choquet D (2012) Regulation of AMPA receptor surface diffusion by PSD-95 slots. Curr Opin Neurobiol 22:453–460.

Rácz B, Blanpied TA, Ehlers MD, Weinberg RJ (2004) Lateral organization of endocytic machinery in dendritic spines. Nat Neurosci 7:917–918.

Rao Y, Ma Q, Vahedi-Faridi A, Sundborger A, Pechstein A, Puchkov D, Luo L, Shupliakov O, Saenger W, Haucke V (2010) Molecular basis for SH3 domain regulation of F-BAR-mediated membrane deformation. Proc Natl Acad Sci USA 107:8213–8218.

Regan P, Piers T, Yi JH, Kim DH, Huh S, Park SJ, Ryu JH, Whitcomb DJ, Cho K (2015) Tau phosphorylation at serine 396 residue is required for hippocampal LTD. J Neurosci 35:4804–4812.

Regan P, Whitcomb DJ, Cho K (2017) Physiological and pathophysiological implications of synaptic tau. Neuroscientist 23:137–151.

Schael S, Nüchel J, Müller S, Petermann P, Kormann J, Pérez-Otaño I, Martínez SM, Paulsson M, Plomann M (2013) Casein kinase 2 phosphorylation of protein kinase C and casein kinase 2 substrate in neurons (PACSIN) 1 protein regulates neuronal spine formation. J Biol Chem 288:9303–9312.

Selkoe DJ (2002) Alzheimer's disease is a synaptic failure. Science 298:789–791.

Stincic TL, Frerking ME (2015) Different AMPA receptor subtypes mediate the distinct kinetic components of a biphasic EPSC in hippocampal interneurons. Front Synaptic Neurosci 7:7.

Suzuki M, Kimura T (2017) Microtubule-associated tau contributes to intradendritic trafficking of AMPA receptors in multiple ways. Neurosci Lett 653:276–282.

Takayasu Y, Iino M, Ozawa S (2004) Roles of glutamate transporters in shaping excitatory synaptic currents in cerebellar Purkinje cells. Eur J Neurosci 19:1285–1295.

Widagdo J, Fang H, Jang SE, Anggono V (2016) PACSIN1 regulates the dynamics of AMPA receptor trafficking. Sci Rep 6:31070.